

PAPER

## Main ion and impurity edge profile evolution across the L- to H-mode transition on DIII-D

To cite this article: S R Haskey *et al* 2018 *Plasma Phys. Control. Fusion* **60** 105001

View the [article online](#) for updates and enhancements.

### Related content

- [Collisionality dependence of edge rotation and in-out impurity asymmetries in ASDEX Upgrade H-mode plasmas](#)  
E. Viezzer, E. Fable, T. Pütterich *et al.*
- [Deuterium charge exchange recombination spectroscopy from the top of the pedestal to the scrape off layer in H-mode plasmas](#)  
S.R. Haskey, B.A. Grierson, L. Stagner *et al.*
- [Intrinsic rotation generation in NSTX ohmic H-mode plasmas](#)  
Jong-Kyu Park, Ronald E. Bell, Stanley M. Kaye *et al.*



**IOP | ebooks™**

Bringing you innovative digital publishing with leading voices to create your essential collection of books in STEM research.

Start exploring the collection - download the first chapter of every title for free.

# Main ion and impurity edge profile evolution across the L- to H-mode transition on DIII-D

S R Haskey<sup>1</sup> , B A Grierson<sup>1</sup> , C Chrystal<sup>2</sup>, A Ashourvan<sup>1</sup>, K H Burrell<sup>2</sup>,  
R J Groebner<sup>2</sup>, E A Belli<sup>2</sup>, L Stagner<sup>3</sup>, D J Battaglia<sup>1</sup> ,  
T Stoltzfus-Dueck<sup>1</sup>  and A Bortolon<sup>1</sup> 

<sup>1</sup> Princeton Plasma Physics Laboratory, Princeton, NJ 08543-0451, United States of America

<sup>2</sup> General Atomics, PO Box 85608, San Diego, CA 92186, United States of America

<sup>3</sup> University of California, Irvine, CA 92697, United States of America

E-mail: [shaskey@pppl.gov](mailto:shaskey@pppl.gov)

Received 4 May 2018, revised 11 July 2018

Accepted for publication 31 July 2018

Published 15 August 2018



CrossMark

## Abstract

Detailed measurements of the main ion ( $D^+$ ) and impurity ion ( $C^{6+}$ ) evolution during the development of the H-mode pedestal across an L–H transition show significant differences in toroidal rotation, density, and temperature profiles in the pedestal region on DIII-D. While both species experience a slow toroidal spin up at constant input neutral beam injected torque, the  $C^{6+}$  toroidal rotation develops a non monotonic notch feature and lower toroidal rotation near the plasma edge immediately following the L–H transition. This feature is not present in the main ion rotation that instead, depending on plasma parameters, can show a flat or peaked rotation near the separatrix. The  $D^+$  and  $C^{6+}$  temperature profiles show a similar evolution; however, the  $D^+$  temperature is lower than the  $C^{6+}$  temperature at the separatrix in both L and H-mode which may be due to cooling of  $D^+$  via charge exchange with cold edge deuterium neutrals. Local neoclassical predictions of the main ion toroidal rotation based on the impurity properties show good agreement with direct measurements at the pedestal top for a lower power, higher collisionality case but can diverge significantly in the steep gradient region for the two shots studied here. These observations highlight the importance of directly measuring the properties of the main ion species at the plasma edge.

Keywords: L–H transition, momentum transport, transport, charge exchange recombination spectroscopy

(Some figures may appear in colour only in the online journal)

## 1. Introduction

Toroidal rotation and its shear play a crucial role in determining stability to large scale MHD [1],  $E \times B$  shear stabilization of micro-turbulence [2], and access to advanced operating scenarios such as ELM suppressed H-mode and QH mode [3, 4]. The continued development and validation of transport models is required to better predict and optimize the toroidal rotation of future magnetic confinement devices such as ITER. This requires improved understanding of topics such as intrinsic rotation [5–9] that depend on accurate measurements of the plasma flow velocity.

The main ion species carries the bulk of the momentum and thermal energy, meaning their temperature, toroidal

velocity, and density are the required measurements for testing momentum and energy transport models. Initial work on making these main ion measurements using charge exchange recombination spectroscopy (CER) in the deuterium neutral beam injection (NBI) heated deuterium plasmas that are typically studied on large tokamaks was performed in the 80s and 90s on T-10 [10], JET [11], and TEXTOR [12]; however, due to the complexities of the spectrum and difficulties modeling the effect of halo emission, the measurements were rarely made and the technique was not developed further until relatively recently [13–19]. Main ion measurements have been made in helium plasmas using CER with deuterium NBI [20, 21]; however, these plasmas suffer from deuterium dilution, and are rarely created due to operational overhead.

Bulk plasma rotation measurements can also be made using Mach probes [22–26]; however due to power flux considerations, these measurements are limited in duration, scenario, and depth into the plasma. Additionally, neutral particle analyzers [27] and collective Thomson scattering [28–30] have been used to measure the main ion properties. Typically, impurity CER [31–34] has been used to determine the properties of an impurity species, usually C-VI( $n = 8 \rightarrow 7$ , 5290.5 Å) on DIII-D, with the main ion properties either being assumed to be equal or inferred using neoclassical models. The main ion and impurity rotation are known to diverge considerably in low collisionality conditions [35, 36] and in regions where there are steep pressure gradients such as the H-mode plasma edge, providing a significant modeling challenge that requires high resolution experimental data for validation.

Advances in CER spectroscopy have allowed direct measurements of the deuterium ion properties in the plasma core [13] and more recently the pedestal and steep gradient region [14–17] in deuterium beam heated plasmas on DIII-D. This technique, referred to as main ion CER (MICER), uses  $D_\alpha$  emission ( $D-I[n = 3 \rightarrow 2, 6561.0 \text{ \AA}]$ ) due to charge exchange with the neutral beams as well as the associated halo emission. Details of how the difficulties of modeling the effect of the halo emission were overcome at the plasma edge using the FIDASIM code [37, 38] are described in [17]. The sight-lines for the edge MICER system are interleaved with sight-lines for the recently upgraded impurity CER system [39] (see figure 1 in [16]) allowing comparisons between the impurities and main ions that are free from spatial uncertainty. This setup allows the simultaneous measurement of the deuterium and impurity temperature, toroidal rotation, and density. The following sections present the results of using this capability to contrast the development of the main ion and impurity pedestals across the L–H transition.

## 2. Profile evolution across L–H transition

Two DIII-D lower single null discharges with favorable  $\nabla B$  direction are investigated. For the first case (164436), a saw-tooth crash triggers an L–H transition, providing an excellent opportunity to study the impurity and main ion properties near the L–H power threshold across the transition while the input beam power and low NBI torque are constant and there are no ELMs. The parameters for this discharge are:  $I_p = 1.3 \text{ MA}$ ,  $B_T = -1.7 \text{ T}$ ,  $P_{\text{NBI}} = 0.8 \text{ MW}$ ,  $T_{\text{NBI}} = 0.9 \text{ N m}$ . Time traces of the central line average density and filterscope signals are shown in figure 1. The integration time for the CER systems is 5 ms, which captures details of the profiles leading up to the L–H transition and the development of the H-mode profiles following the transition, but is not fast enough to capture details of the transition event. The plasma impurity content is low in this plasma, with an effective plasma charge  $Z_{\text{eff}} \approx 1.2$ . The second discharge (164988) is a near zero input torque ITER baseline scenario [40] with the following parameters:  $I_p = 1.2 \text{ MA}$ ,  $B_T = -2.0 \text{ T}$ ,  $P_{\text{NBI}} = 4 \text{ MW}$ ,  $T_{\text{NBI}} = 0.2 \text{ N m}$ . This discharge has four times the beam heating compared with

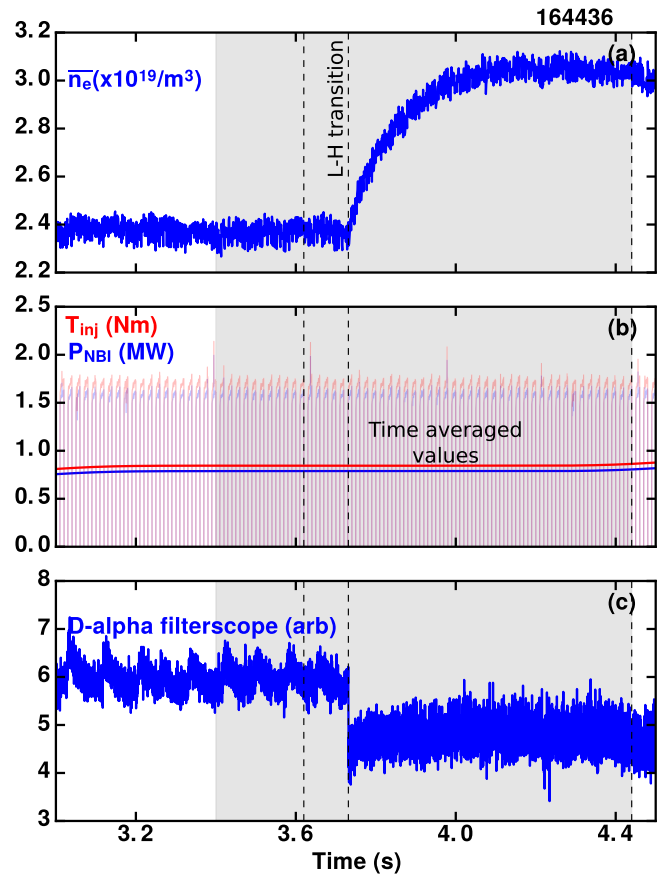


**Figure 1.** Time evolution of the central line averaged density (a), and power and torque (b), across an L–H transition which occurs at 3731 ms. Smoothed values of the power and torque are also shown. Rapid changes in the density (a) are concomitant with the reduction in edge  $D_\alpha$  (c). The shaded region and vertical dashed lines at 3620 and 4440 ms are investigated in subsequent figures.

the first case and is more representative of a typical high performance H-mode on DIII-D. For this case, the H-mode profiles are compared. These two cases are referred to as the ‘low power case’ and ‘ITER baseline case’ in the rest of the paper. Large portions of the data analysis shown in this work were performed using the OMFIT [41] modeling framework using the OMFITprofiles and TRANSP modules [42, 43].

### 2.1. Toroidal rotation evolution

Evolution of the toroidal rotation profiles provides insight into the nature of the transport changes across a confinement transition. Rotation profiles for  $D^+$  and  $C^{6+}$  across the L–H transition (marked in figure 1 for the low power case) are shown in figures 2(a) and (b) respectively. Profiles are plotted against  $\rho$ , the square-root of normalized toroidal magnetic flux. Inside the top of the pedestal both species show an increase of the toroidal rotation at near constant input beam torque as the plasma achieves an increased angular momentum, but species dependent modifications are seen in the pedestal and steep gradient region.

Contrasting the main ion and impurity toroidal rotation exposes key qualitative differences that deviate from

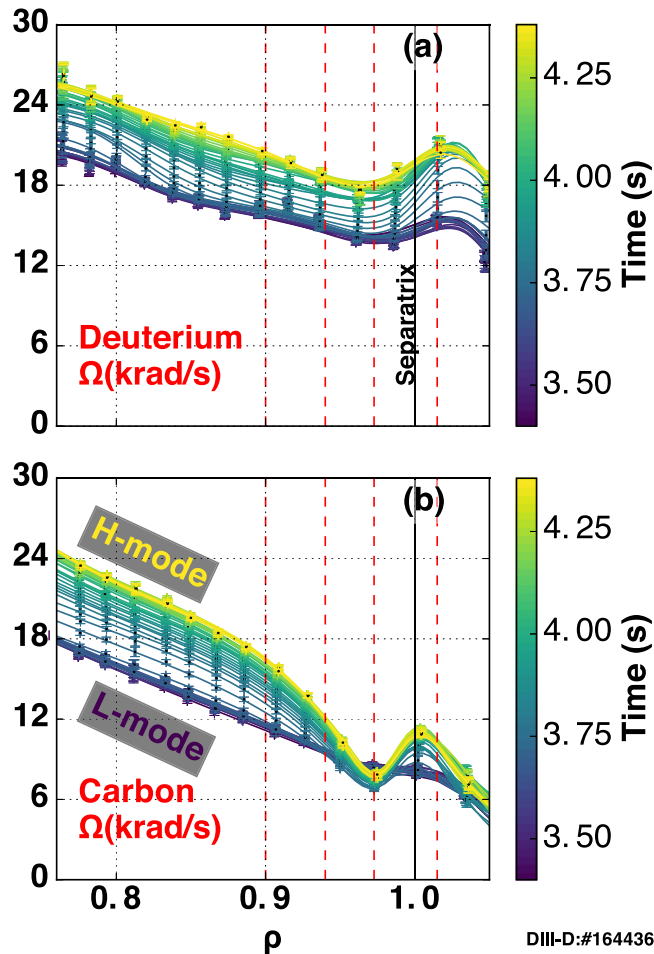


**Figure 2.** Rotation profile evolution of  $D^+$  (a) and  $C^{6+}$  (b) across the L–H transition marked in figure 1 plotted against the square-root of normalized toroidal magnetic flux ( $\rho$ ). A notch develops very rapidly in the  $C^{6+}$  rotation just inside the separatrix. This feature is not present in the main ion rotation. Time histories at the location of the vertical red dashed lines are shown in figure 3.

expectations of reduced transport in the steep gradient region due to  $E \times B$  shear suppression of turbulent transport. The main ion rotation profile remains relatively flat, which is not expected if the momentum flux obeys Fick’s law and the momentum diffusivity is reduced. Instead, the increased rotation at the top of the pedestal appears to be due to the increase in the toroidal rotation boundary condition at the separatrix.

In contrast to the main ion rotation, the impurity rotation develops sharp gradients in the pedestal; however, this is not in the manner expected from reduced momentum diffusion. Rather than displaying a standard transport barrier with increasing magnitude of a monotonic profile gradient, the impurity rotation profile exhibits both an increasing negative gradient on the core side of the pedestal following the L–H transition, and a positive gradient on the separatrix side of the pedestal.

Similar notch features have been observed previously in impurity toroidal rotation measurements on ASDEX upgrade [21, 44–46], DIII-D [47, 48], and TFTR [49]. In the ASDEX work the notch is in the pedestal region and was attributed to

an impurity density asymmetry with higher concentrations on the high field side. On TFTR high performance supershot discharges a notch was observed near the core, in regions of high ion temperature gradients and was attributed to anomalous radial momentum diffusion together with parallel heat friction on the impurity ions due to neoclassical parallel heat flow [49]. The same work used neoclassical calculations to predict that the notch is not present in the main ion toroidal rotation allowing for a profile consistent with anomalous radial diffusion of toroidal momentum. A clear result of the new measurements shown in this paper is that the notch is not visible in the bulk main ion toroidal rotation.

In order to better see the time evolution of the notch feature, figure 3(c) shows time traces of the toroidal rotation for  $C^{6+}$  and  $D^+$  at  $\rho = 0.97$ . The individual impurity and main ion channel measurements are linearly interpolated in  $\rho$  to provide time traces which are at constant  $\rho$  values. The notch develops faster than the 5 ms integration time of the CER measurement indicating that if the notch is due to impurity density asymmetries, they develop within 5 ms of the L–H transition.

The time evolution can be separated into a prompt initial behavior which occurs within 5 ms of the L–H transition and a longer timescale evolution towards the saturated values. Comparing figures 3(a)–(d) we can see that the main ion toroidal rotation increases across all shown  $\rho$  values following the L–H transition while the carbon shows an opposite behavior around the notch feature ( $\rho = 0.97$ ). The main ion toroidal rotation evolution towards the saturated value is slower than the main ion temperature and density evolution, which are also shown in figure 3 and discussed in the following sections. Detailed toroidal rotation profiles and comparisons with neoclassical theory for the low power case and ITER baseline case are described in section 2.4.

## 2.2. Temperature

It is well known that the temperature of the electrons and commonly measured impurity ions can differ significantly depending on how the plasma is heated and the dominant energy transport mechanisms. Differences between the impurity and main ion temperatures have received much less attention, largely due to the absence of main ion temperature measurements in  $D^+$  plasmas and the assumption that they are typically well coupled. The ion temperatures are often assumed to be equal in the absence of direct  $D^+$  temperature measurements. This assumption has implications in areas such as pedestal stability analysis, ITG turbulence drive, and provides a boundary condition for ion energies in scrape off layer studies. The observed differences between the  $D^+$  and  $C^{6+}$  temperatures for the two shots studied in this paper are described below.

Figure 4 compares the species dependent toroidal rotation and temperature profiles for the low power case before (a), (c) and after (b), (d) the L–H transition. In L-mode (figure 4(c)) both the  $C^{6+}$  and  $D^+$  ion temperatures are well coupled within the error bars except near the separatrix where the difference increases slightly. In the lower collisionality

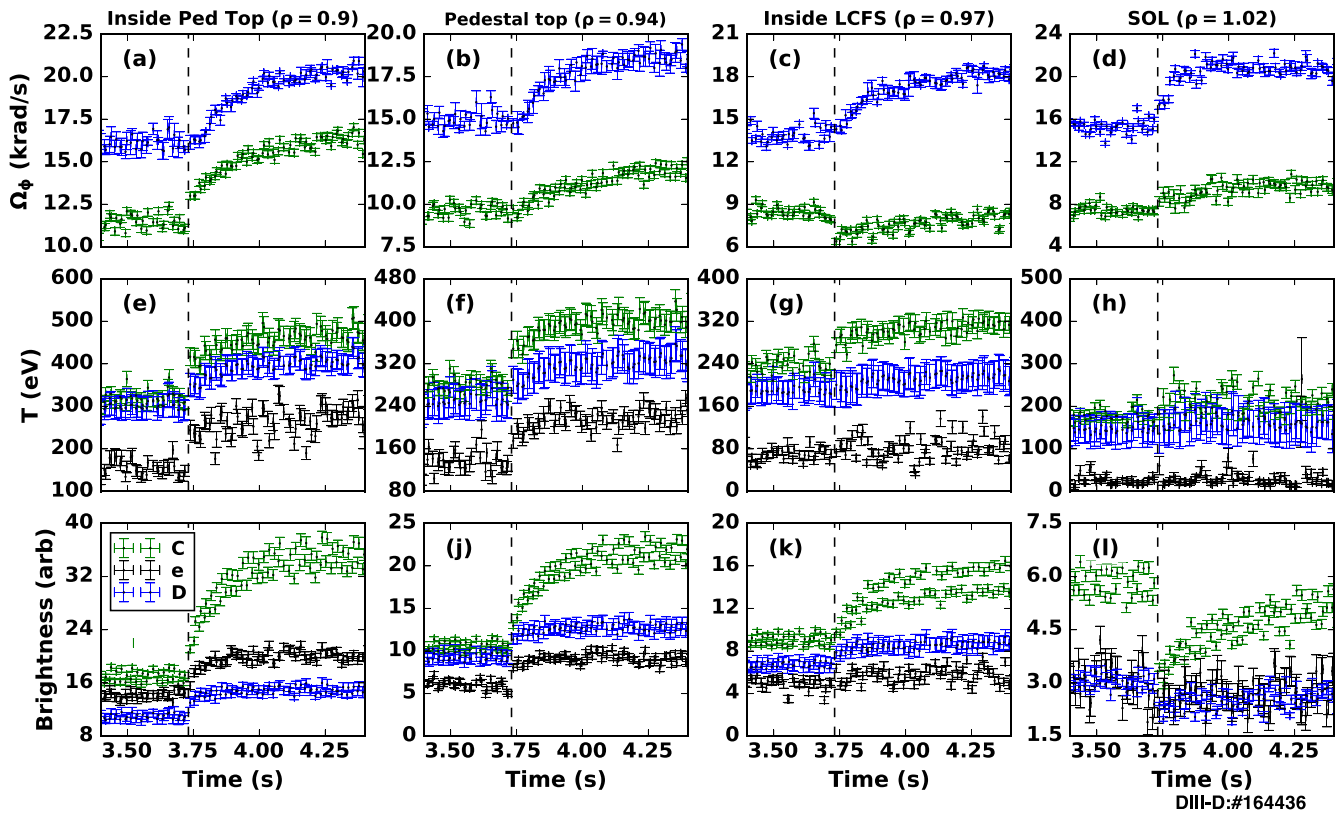


**Figure 3.** Time traces of the  $C^{6+}$  (green) and  $D^{+}$  (blue) toroidal rotation (top row), temperature (middle row) and brightness (bottom row) across the L–H transition, which is marked with the vertical dashed line. The brightness is approximately proportional to particle density. The electron (black) temperature and density are shown in the middle and bottom rows respectively, with the density being scaled to fit on the same axis as the brightness. The rows do not share the same axis and are zero suppressed so that the dynamics can be seen more clearly. Each column represents a different radial location that is marked by the red dashed lines in figure 2.

H-mode (figure 4(d)) for the same shot, the differences between the two species increases with the  $D^{+}$  temperature being approximately 70 eV lower, halfway between the  $C^{6+}$  and electron temperatures.

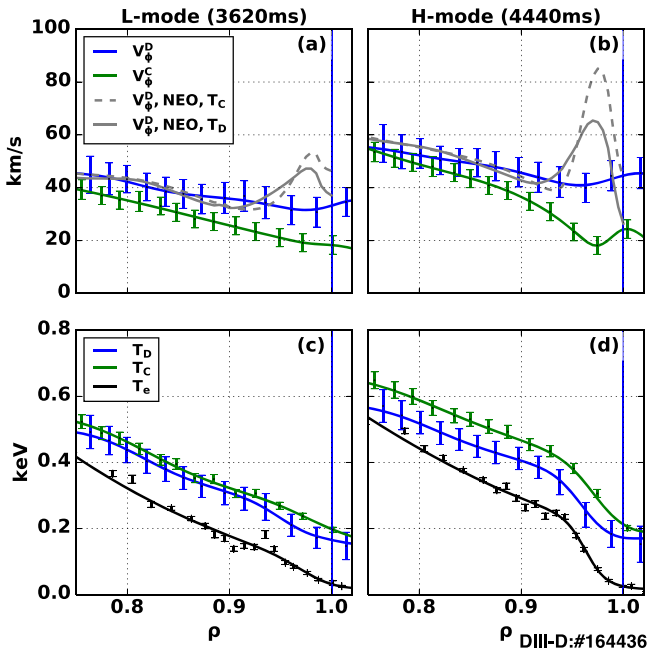
One possibility for the difference between the apparent main ion and impurity temperatures inside the top of the pedestal is the effect that Zeeman splitting can have on the observed temperature. Calculations using the parameterization in [50] show that this effect is negligible for the main ions, but may be significant for the impurity ions, reducing the temperature difference by  $\approx 30$  eV for the cases shown here. However, this parameterization assumes that the upper energy levels are statistically populated which is not the case for active charge exchange due to the  $l$ -dependent cross-sections, so it is not applied to the plots shown here and further investigation is left as future work.

Figure 5 shows species dependent temperature and toroidal rotation plots for the ITER baseline case in H-mode. Similar differences (compared with the low power case) are seen for the temperatures inside the top of the pedestal (figure 5(b)); however, as the separatrix is approached the difference between the  $C^{6+}$  and  $D^{+}$  temperatures increases rapidly with the main ion temperature being less than half the  $C^{6+}$  temperature near the separatrix. Some possible reasons for the differences near the separatrix include the effects of in–out impurity density asymmetries, banana orbit widths of

higher energy tail impurity ions, and atomic physics considerations. Additionally, at the separatrix the main ion temperature is 2–3 times higher than the electron temperature. This is roughly consistent with other experimental measurements [51] and conventional models of SOL heat transport for low collisionality [52].

As was described in the previous section, the existence of a notch in the impurity toroidal rotation profile may signify in–out impurity density asymmetries that have been measured on both ASDEX upgrade [45] and CMOD [53] using high field side gas puff CER. As discussed in the CMOD work [53], if the pressure is constant on a flux surface, then the existence of a higher impurity density on the high field side means that the temperature on the low field side will be higher than the flux surface averaged temperature. This could partially explain the elevated impurity temperature relative to the main ion temperature on the low field side.

There are also important atomic physics considerations near the separatrix where multiple charge states of carbon exist. It is important to note that there are six positive charge states for carbon and we are only measuring the fully ionized one. The ionization energy for  $C^{5+}$  is 490 eV, which is significantly larger than the electron temperatures near the plasma edge, meaning that there will be significant distributions of lower charge states of carbon. This reduction in



**Figure 4.**  $C^{6+}$  and  $D^+$  toroidal rotation and temperature profiles in L-mode and H-mode. Predictions of the main ion toroidal rotation using NEO show accurate predictions of the increased  $D^+$  velocity relative to the  $C^{6+}$  inside the pedestal top but significant differences in the steep gradient region. There are two NEO predictions: one uses the newly measured main ion measurement, the second assumes that the main ion temperature is the same as the  $C^{6+}$  temperature which is commonly assumed in the absence of  $D^+$  temperature measurements.

$C^{6+}$  density near the separatrix means that the  $C^{6+}$  that exists there will have a larger proportion of higher energy tail ions from deeper inside the plasma which are on the co-current leg of their banana orbits, leading to an increase in the measured temperature. This effect was simulated using XGC0 for a QH mode (see figure 3(d) in [54]) and reproduced the observed increase in impurity temperature in the scrape off layer. This increase in impurity temperature crossing the separatrix is also seen in figure 5(b).

Another consideration is that the interaction with the cold deuterium neutrals at the plasma edge will have a direct cooling effect on the  $D^+$  population but not the  $C^{6+}$ . Charge exchange between a thermal  $D^+$  and cold deuterium neutral essentially swaps a hot  $D^+$  for a cold  $D^+$  reducing the overall temperature of the  $D^+$  population (modeling of the cooling effect of edge cold neutrals on the  $D^+$  and associated effects on ITG turbulence is discussed in [55]). On the other hand, charge exchange between a thermal  $C^{6+}$  and a cold deuterium produces a  $C^{5+}$  and a cold  $D^+$ , which reduces the  $C^{6+}$  density but does not affect its temperature (a new  $C^{6+}$  is not created). Because this process creates a cold  $D^+$ , it also reduces the temperature of the  $D^+$  population. In summary these considerations mean that the interaction with the cold edge deuterium neutrals is a thermal sink for  $D^+$  but not the  $C^{6+}$ .

The time traces of the impurity, main ion temperature, and electron temperature at different radial locations across the L–H transition are shown in the middle row of figure 3. A sudden jump is seen in the temperatures of all three species at

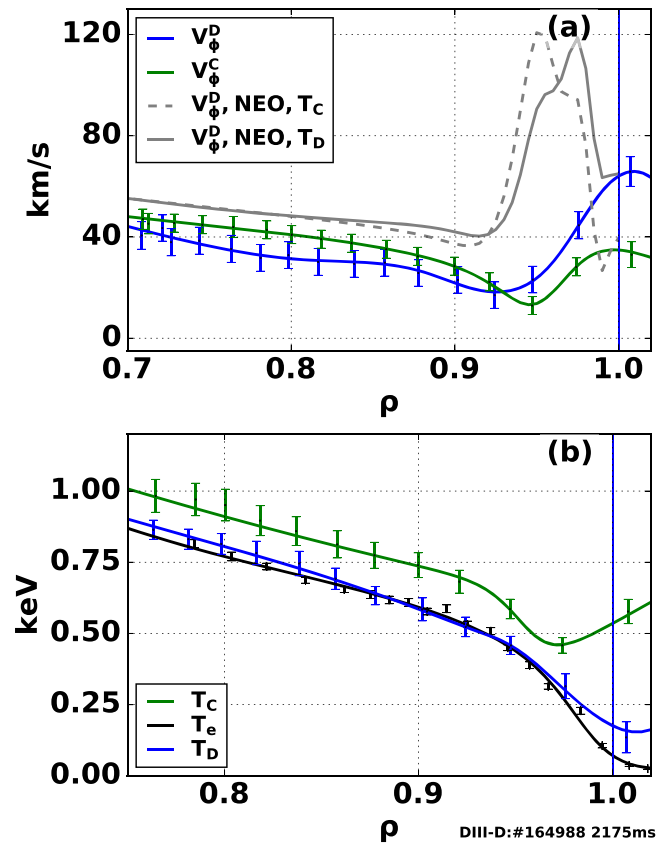


**Figure 5.** Toroidal rotation and temperature profiles for  $\approx 0$  N m input torque, high performance ITER baseline scenario H-mode which has a factor of 4 higher injected power compared with the discharge shown in previous figures.

the pedestal top following the L–H transition event on the prompt 5 ms timescale along with an increased difference between the  $C^{6+}$  and  $D^+$  temperatures. On a longer time-scale, the edge main ion temperature does not change significantly while the toroidal rotation shows significant spin up. Additionally, the main ion temperature evolves more rapidly towards its saturated value than the toroidal rotation, demonstrating that the changes in energy and momentum transport following the L–H transition are not the same.

### 2.3. Particle density

The evolution of the brightness of the thermal charge exchange line is shown in the bottom row of figure 3. The emission brightness is proportional to the charge exchange cross section, the neutral beam density and the density of the ions being measured. The first two terms are approximately constant across the edge region, meaning that brightness provides a good proxy for changes in the particle densities of the impurities and main ions in the edge region. The electron density is also shown in these plots with an appropriate scaling to fit on the same axes.

As with the temperature (and contrasted against the main ion toroidal rotation), rapid changes are seen immediately following the L–H transition within the 5 ms integration time of these measurements. This is most clear for the impurities in

the scrape off layer (figure 3(l)) where the  $C^{6+}$  brightness immediately decreases by a factor of two indicating a dramatic change in the impurity particle transport. The cause of this rapid change may be due to the following: a decrease in outward impurity particle flux due to the formation of the transport barrier, an increase in the inward particle pinch, and/or a possible poloidal redistribution of the impurities.

Both the main ion brightness and electron density evolve more rapidly to their steady state values compared with the impurities. The density of the impurities increases by a factor of  $\approx 2$  for the locations inside the plasma compared with a factor of  $\approx 1.4$  for the main ions. The drop in divertor  $D_\alpha$  light following the L–H transition demonstrates a reduction in the plasma density in the scrape off layer, consequently the neutrals can penetrate further into the plasma increasing the  $D^+$  source further inside the plasma, which may play a role in the more rapid evolution of the  $D^+$  density [56]. The longer evolution of the  $C^{6+}$  has a minor impact on the electron density evolution because  $Z_{\text{eff}}$  is low in this plasma.

#### 2.4. L and H-mode toroidal rotation profiles and comparison with neoclassical theory

The difference between the  $C^{6+}$  and  $D^+$  toroidal rotation increases significantly near the separatrix with the  $D^+$  rotating more rapidly, as shown in figure 4 for the low power case and in figure 5 for the ITER baseline discharge, which has a factor of 4 higher injected power. The difference between the two species increases going from L-mode (low power case) to H-mode (low power case) to the ITER baseline case where there is a rapid  $60 \text{ km s}^{-1}$  co-current peaked toroidal rotation at the separatrix. When interpreting these toroidal rotation measurements it is important to note that these measurements are made at the low field side midplane and are not flux surface averaged quantities. This edge rotation feature may be due to ion orbit shifts, as treated in ion orbit loss models [57, 58], first-order neoclassical flows, or transport-driven edge rotation [9] and it may be a signature of intrinsic rotation generation mechanism. The origin and transport of this edge rotation is an active area of research that has been investigated using Mach probes [26, 59]. Simulations have been performed with full function gyrokinetic XGC1 modeling [60] and kinetic neoclassical XGC0 modeling for a QH mode case [54, 61].

In low  $Z_{\text{eff}}$  plasmas, the toroidal momentum is dominated by the main ions; consequently momentum transport studies rely on the main ion toroidal rotation. In the absence of direct main ion toroidal rotation measurements, neoclassical calculations of poloidal velocity are often used to obtain the main ion toroidal rotation. We can test this workflow using the main ion toroidal rotation measurements for the two cases studied in this paper. Neoclassical codes cannot directly calculate the main ion toroidal rotation. Instead they calculate the neoclassical main ion poloidal rotation and use this value in the radial force balance relation along with the radial electric field, main ion density, and temperature profiles to obtain the main ion toroidal rotation. The radial electric field is usually measured experimentally through impurity CER measurements of

the impurity toroidal and poloidal rotation as well as impurity density and temperature profiles. If the impurity poloidal rotation measurement is not available, the neoclassical impurity poloidal rotation can be calculated and used with the other profiles to obtain a ‘neoclassical’ radial electric field.

Figures 4(a), (b) and 5(a) show the results from performing this calculation using NEO [62] which is a  $\delta f$  Eulerian model that solves the drift-kinetic equation in a multi-ion species plasma. Here, NEO is used to calculate the poloidal rotation of both the main ions and impurities. The calculations are shown for the case where the main ion temperature is assumed to be equal to the impurity ion temperature (a typical assumption when main ion temperature measurements are not available), and where the respective temperatures for each species are provided as inputs. The agreement is slightly better when the respective temperatures are used. For both the L and H-mode in the low power case, good agreement is found for  $\rho < 0.93$ . However, at the very edge of the plasma ( $\rho > 0.93$ ) significant differences are found. For the higher powered ITER baseline case, large differences are seen in the steep gradient region, along with a systematic  $\approx 15 \text{ km s}^{-1}$  offset between the measurements and neoclassical predictions for  $\rho < 0.9$ . These discrepancies mean that there are differences between the poloidal rotations and those predicted by NEO. These differences may be the result of increased finite orbit width effects in the steep gradients, ion orbit loss effects, or due to the interaction with neutrals, which are not included in the NEO code. Comparison with modeling using codes that include some of these effects [54, 61], at significantly greater computational cost, is ongoing.

The question of whether poloidal rotation can be explained by neoclassical theory has been the subject of significant work, with mixed results [20, 21, 35, 63–68]. Extensive comparisons between neoclassical calculations of main ion poloidal rotation, and the inferred main ion poloidal rotation at the plasma edge (using the measured radial electric field and the main ion properties, as described for core MICER measurements in [35]) will be the subject of future work.

### 3. Conclusions

MICER along with standard impurity CER has been used to study the differences between the  $C^{6+}$  and  $D^+$  temperature, toroidal rotation, and density evolution across an L–H transition at the plasma edge. Large differences are seen in both the magnitude and profile shape of the  $C^{6+}$  and  $D^+$  toroidal rotation before and after the L–H transition in the steep gradient region of deuterium plasmas heated with deuterium NBI. The  $D^+$  can be rotating significantly faster than the  $C^{6+}$  with a large co-current peak near the separatrix seen for high power 0 Nm torque ITER baseline scenario. Neoclassical predictions of the main ion poloidal rotation, which are often used to calculate the main ion toroidal rotation in the absence of direct measurements can provide a good prediction at the pedestal top for some cases, but large differences are seen in the steep gradient region.

The main ion temperature can be as low as half the value of the commonly measured impurity ion temperature at the separatrix, most likely due to atomic physics effects cooling the deuterium at the plasma edge. Both the main ion temperature and density are shown to increase on a much faster timescale to their saturated values than the toroidal rotation following the L–H transition. These observations highlight the importance of directly measuring the properties of the main ion species at the plasma edge.

#### 4. Disclaimer

This report was prepared as an account of work sponsored by an agency of the United States Government. Neither the United States Government nor any agency thereof, nor any of their employees, makes any warranty, express or implied, or assumes any legal liability or responsibility for the accuracy, completeness, or usefulness of any information, apparatus, product, or process disclosed, or represents that its use would not infringe privately owned rights. Reference herein to any specific commercial product, process, or service by trade name, trademark, manufacturer, or otherwise, does not necessarily constitute or imply its endorsement, recommendation, or favoring by the United States Government or any agency thereof. The views and opinions of authors expressed herein do not necessarily state or reflect those of the United States Government or any agency thereof.

#### Acknowledgments

This material is based upon work supported by the US Department of Energy, Office of Science, Office of Fusion Energy Sciences, using the DIII-D National Fusion Facility, a DOE Office of Science user facility under Grants No. DE-AC02-09CH11466 (Princeton University), No. DE-FC02-04ER54698, and DE-FC02-95ER54309 (General Atomics). DIII-D data shown in this paper can be obtained in digital format by following the links at [https://fusion.gat.com/global/D3D\\_DMP](https://fusion.gat.com/global/D3D_DMP).

#### ORCID iDs

S R Haskey  <https://orcid.org/0000-0002-9978-6597>  
 B A Grierson  <https://orcid.org/0000-0001-5918-6506>  
 D J Battaglia  <https://orcid.org/0000-0001-8897-9740>  
 T Stoltzfus-Dueck  <https://orcid.org/0000-0003-2587-6298>  
 A Bortolon  <https://orcid.org/0000-0002-0094-0209>

#### References

- [1] Garofalo A M, Strait E J, Johnson L C, La Haye R J, Lazarus E A, Navratil G A, Okabayashi M, Scoville J T, Taylor T S and Turnbull A D 2002 Sustained stabilization of the resistive-wall mode by plasma rotation in the DIII-D tokamak *Phys. Rev. Lett.* **89** 235001
- [2] Burrell K H 1997 Effects of [formula omitted] velocity shear and magnetic shear on turbulence and transport in magnetic confinement devices *Phys. Plasmas* **4** 1499–518
- [3] Garofalo A M *et al* 2011 Advances towards QH-mode viability for ELM-stable operation in ITER *Nucl. Fusion* **51** 083018
- [4] Burrell K H *et al* 2016 Discovery of stationary operation of quiescent H-mode plasmas with net-zero neutral beam injection torque and high energy confinement on DIII-D *Phys. Plasmas* **23** 056103
- [5] Rice J E 2016 Experimental observations of driven and intrinsic rotation in tokamak plasmas *Plasma Phys. Control. Fusion* **58** 083001
- [6] Ashourvan A, Grierson B A, Battaglia D J, Haskey S R and Stoltzfus-Dueck T 2018 Validation of the kinetic-turbulent-neoclassical theory for edge intrinsic rotation in DIII-D *Phys. Plasmas* **25** 056114
- [7] Chrystal C, Grierson B A, Staebler G M, Petty C C, Solomon W M, DeGrassie J S, Burrell K H, Tala T and Salmi A 2017 Predicting rotation for ITER via studies of intrinsic torque and momentum transport in DIII-D *Phys. Plasmas* **24** 056113
- [8] Chrystal C, Grierson B A, Solomon W M, Tala T, DeGrassie J S, Petty C C, Salmi A and Burrell K H 2017 Dependence of intrinsic torque and momentum confinement on normalized gyroradius and collisionality in the DIII-D tokamak *Phys. Plasmas* **24** 042501
- [9] Stoltzfus-Dueck T 2012 Transport-driven toroidal rotation in the tokamak edge *Phys. Rev. Lett.* **108** 065002
- [10] Berezovskij E, Berezovskaya M, Izvozchikov A, Krupin V and Rantsev-Kartinov V 1985 Local ion temperature measurements from Doppler broadening of hydrogen lines using a fast atomic beam *Nucl. Fusion* **25** 1495–8
- [11] Mandl W 1992 Development of active Balmer-alpha spectroscopy at JET *Technical Report JET-IR(92)05* JET
- [12] Busche E, Euringer H and Jaspers R 1997 Measurement of deuterium ion temperature profiles at TEXTOR-94 *Plasma Phys. Control. Fusion* **39** 1327–38
- [13] Grierson B A, Burrell K H, Chrystal C, Groebner R J, Kaplan D H, Heidbrink W W, Muñoz Burgos J M, Pablant N A, Solomon W M and Van Zeeland M A 2012 Active spectroscopic measurements of the bulk deuterium properties in the DIII-D tokamak (invited) *Rev. Sci. Instrum.* **83** 10D529(6)
- [14] Haskey S R *et al* 2018 Active spectroscopy measurements of the deuterium temperature, rotation, and density from the core to scrape off layer on the DIII-D tokamak (invited) *Rev. Sci. Instrum.* (<https://doi.org/10.1063/1.5038349>)
- [15] Haskey S R, Grierson B A, Burrell K H, Chrystal C, Groebner R J, Kaplan D H, Pablant N A and Stagner L 2016 Measurement of deuterium density profiles in the H-mode steep gradient region using charge exchange recombination spectroscopy on DIII-D *Rev. Sci. Instrum.* **87** 11E553
- [16] Grierson B A, Burrell K H, Chrystal C, Groebner R J, Haskey S R and Kaplan D H 2016 High resolution main-ion charge exchange spectroscopy in the DIII-D H-mode pedestal *Rev. Sci. Instrum.* **87** 11E545
- [17] Haskey S R, Grierson B A, Stagner L, Burrell K H, Chrystal C, Groebner R J, Ashourvan A and Pablant N A 2017 Deuterium charge exchange recombination spectroscopy from the top of the pedestal to the scrape off layer in H-mode plasmas *J. Instrum.* **12** C10013
- [18] Salewski M *et al* 2018 Deuterium temperature, drift velocity, and density measurements in non-Maxwellian plasmas at ASDEX Upgrade *Nucl. Fusion* **58** 036017
- [19] Krupin V A *et al* 2013 Charge-exchange recombination spectroscopy of the plasma ion temperature at the T-10 tokamak *Plasma Phys. Rep.* **39** 632–43

- [20] Kim J, Burrell K H, Gohil P, Groebner R J, Kim Y B, John H E St, Seraydarian R P and Wade M R 1994 Rotation characteristics of main ions and impurity ions in H-mode tokamak plasma *Phys. Rev. Lett.* **72** 2199–202
- [21] Viezzer E *et al* 2015 Collisionality dependence of edge rotation and in–out impurity asymmetries in ASDEX Upgrade H-mode plasmas *Nucl. Fusion* **55** 123002
- [22] Labombard B *et al* 2004 Transport-driven Scrape-off-layer flows and the boundary conditions imposed at the magnetic separatrix in a tokamak plasma *Nucl. Fusion* **44** 1047–66
- [23] Labombard B *et al* 2008 Critical gradients and plasma flows in the edge plasma of Alcator C-Mod *Phys. Plasmas* **15** 056106
- [24] Erents S K, Chankin A V, Matthews G F and Stangeby P C 2000 Parallel flow in the JET scrape-off layer *Plasma Phys. Control. Fusion* **42** 905–15
- [25] Asakura N, Sakurai S, Hosogane N, Shimada M, Itami K, Koide Y and Naito O 1999 Heat and particle transport of SOL and divertor plasmas in the W shaped divertor on JT-60U *Nucl. Fusion* **39** 1983–94
- [26] Boedo J A *et al* 2016 Experimental evidence of edge intrinsic momentum source driven by kinetic ion loss and edge radial electric fields in tokamaks *Phys. Plasmas* **23** 092506
- [27] Romannikov A, Bourdelle C, Bucalossi J, Hutter T, Platz P and Saint-Laurent F 2000 Measurement of central toroidal rotation in ohmic Tore Supra plasmas *Nucl. Fusion* **40** 319–24
- [28] Nishiura M *et al* 2014 Spectrum response and analysis of 77 GHz band collective Thomson scattering diagnostic for bulk and fast ions in LHD plasmas *Nucl. Fusion* **54** 023006
- [29] Stejner M *et al* 2017 Main-ion temperature and plasma rotation measurements based on scattering of electron cyclotron heating waves in ASDEX Upgrade *Plasma Phys. Control. Fusion* **59** 075009
- [30] Abramovic I, Pavone A, Svensson J, Moseev D, Salewski M, Laqua H P, Cardozo N J and Wolf R C 2017 Collective Thomson scattering data analysis for Wendelstein 7-X *J. Instrum.* **12** C08015
- [31] Fonck R J, Goldston R J, Kaita R and Post D E 1983 Plasma ion temperature measurements via charge exchange recombination radiation *Appl. Phys. Lett.* **42** 239–41
- [32] Fonck R J, Darrow D S and Jaehnig K P 1984 Determination of plasma-ion velocity distribution via charge-exchange recombination spectroscopy *Phys. Rev. A* **29** 3288–309
- [33] Isler R C 1994 An overview of charge-exchange spectroscopy as a plasma diagnostic *Plasma Phys. Control. Fusion* **36** 171–208
- [34] Groebner R J, Brooks N H, Burrell K H and Rottler L 1983 Measurements of plasma ion temperature and rotation velocity using the He II 4686-Å line produced by charge transfer *Appl. Phys. Lett.* **43** 920–2
- [35] Grierson B A, Burrell K H, Solomon W M, Budny R V and Candy J 2013 Collisionality scaling of main-ion toroidal and poloidal rotation in low torque DIII-D plasmas *Nucl. Fusion* **53** 063010
- [36] Grierson B A, Burrell K H, Heidbrink W W, Lanctot M J, Pablant N A and Solomon W M 2012 Measurements of the deuterium ion toroidal rotation in the DIII-D tokamak and comparison to neoclassical theory *Phys. Plasmas* **19** 056107
- [37] Heidbrink W W, Liu D, Luo Y, Ruskov E and Geiger B 2011 A code that simulates fast-ion  $D\alpha$  and neutral particle measurements *Commun. Comput. Phys.* **10** 716–41
- [38] Stagner L, Geiger B and Heidbrink W W 2016 FIDASIM: a neutral beam and fast-ion diagnostic modeling suite (<https://doi.org/10.5281/zenodo.1341369>)
- [39] Chrystal C, Burrell K H, Grierson B A, Haskey S R, Groebner R J, Kaplan D H and Briesemeister A 2016 Improved edge charge exchange recombination spectroscopy in DIII-D *Rev. Sci. Instrum.* **87** 11E512
- [40] Doyle E J *et al* 2010 Demonstration of ITER operational scenarios on DIII-D *Nucl. Fusion* **50** 075005
- [41] Meneghini O *et al* 2015 Integrated modeling applications for tokamak experiments with OMFIT *Nucl. Fusion* **55** 083008
- [42] Logan N C, Grierson B A, Haskey S R, Smith S P, Meneghini O and Eldon D 2018 OMFIT tokamak profile data fitting and physics analysis *Fusion Sci. Technol.* **74** 125–34
- [43] Grierson B A *et al* 2018 Orchestrating TRANSP simulations for interpretative and predictive tokamak modeling with OMFIT *Fusion Sci. Technol.* **74** 101–15
- [44] Pütterich T, Wolfrum E, Dux R and Maggi C F 2009 Evidence for strong inversed shear of toroidal rotation at the edge-transport barrier in the ASDEX upgrade *Phys. Rev. Lett.* **102** 025001
- [45] Pütterich T, Viezzer E, Dux R and McDermott R M 2012 Poloidal asymmetry of parallel rotation measured in ASDEX Upgrade *Nucl. Fusion* **52** 083013
- [46] Viezzer E *et al* 2017 Investigation of inter-ELM ion heat transport in the H-mode pedestal of ASDEX Upgrade plasmas *Nucl. Fusion* **57** 022020
- [47] deGrassie J S, Burrell K H, Baylor L R, Houlberg W and Lohr J 2004 Toroidal rotation in DIII-D in electron cyclotron heating and Ohmic H-mode discharges *Phys. Plasmas* **11** 4323–31
- [48] deGrassie J S, Rice J E, Burrell K H, Groebner R J and Solomon W M 2007 Intrinsic rotation in DIII-D *Phys. Plasmas* **14** 056115
- [49] Ernst D R *et al* 1998 Notched velocity profiles and the radial electric field in high ion temperature plasmas in the tokamak fusion test reactor *Phys. Plasmas* **5** 665–81
- [50] Blom A and Jupén C 2002 Parametrization of the Zeeman effect for hydrogen-like spectra in high-temperature plasmas *Plasma Phys. Control. Fusion* **44** 312
- [51] Brunner D *et al* 2013 An assessment of ion temperature measurements in the boundary of the Alcator C-Mod tokamak and implications for ion fluid heat flux limiters *Plasma Phys. Control. Fusion* **55** 095010
- [52] Stangeby P 2000 *Plasma Physics and Controlled Fusion (Series in Plasma Physics vol 43)* (Boca Raton, FL: CRC Press) pp 223–4
- [53] Churchill R M *et al* 2015 Poloidal asymmetries in edge transport barriers *Phys. Plasmas* **22** 056104
- [54] Battaglia D J, Burrell K H, Chang C S, Ku S, Degraessie J S and Grierson B A 2014 Kinetic neoclassical transport in the H-mode pedestal *Phys. Plasmas* **21** 072508
- [55] Stotler D P, Lang J, Chang C S, Churchill R M and Ku S 2017 Neutral recycling effects on ITG turbulence *Nucl. Fusion* **57** 086028
- [56] Rensink M E, Allen S L, Futch A H, Hill D N, Porter G D and Mahdavi M A 1993 Particle transport studies for single-null divertor discharges in DIII-D *Phys. Fluids B* **5** 2165–75
- [57] Chang C S, Ku S and Weitzner H 2004 Numerical study of neoclassical plasma pedestal in a tokamak geometry *Phys. Plasmas* **11** 2649–67
- [58] deGrassie J S, Müller S H and Boedo J A 2012 Plasma flow due to a loss-cone distribution centred around the outboard edge in DIII-D *Nucl. Fusion* **52** 013010
- [59] Müller S H, Boedo J A, Burrell K H, Degraessie J S, Moyer R A, Rudakov D L, Solomon W M and Tynan G R 2011 Intrinsic rotation generation in ELM-free H-mode plasmas in the DIII-D tokamak-experimental observations *Phys. Plasmas* **18** 072504
- [60] Seo J, Chang C S, Ku S, Kwon J M, Choe W and Müller S H 2014 Intrinsic momentum generation by a combined neoclassical and turbulence mechanism in diverted DIII-D plasma edge *Phys. Plasmas* **21** 092501
- [61] Battaglia D J, Burrell K H, Chang C S, Degraessie J S, Grierson B A, Groebner R J and Hager R 2016 Improved

- kinetic neoclassical transport calculation for a low-collisionality QH-mode pedestal *Plasma Phys. Control. Fusion* **58** 085009
- [62] Belli E A and Candy J 2008 Kinetic calculation of neoclassical transport including self-consistent electron and impurity dynamics *Plasma Phys. Control. Fusion* **50** 095010
- [63] Solomon W M, Burrell K H, Andre R, Baylor L R, Budny R, Gohil P, Groebner R J, Holcomb C T, Houlberg W A and Wade M R 2006 Experimental test of the neoclassical theory of impurity poloidal rotation in tokamaks *Phys. Plasmas* **13** 056116
- [64] Chrystal C *et al* 2014 Testing neoclassical and turbulent effects on poloidal rotation in the core of DIII-D *Phys. Plasmas* **21** 072504
- [65] Bell R E, Levinton F M, Batha S H, Synakowski E J and Zarnstorff M C 1998 Poloidal rotation in tfr reversed shear plasmas *Phys. Rev. Lett.* **81** 1429–32
- [66] Lebschy A *et al* 2018 Measurement of the complete core plasma flow across the LOC-SOC transition at ASDEX Upgrade *Nucl. Fusion* **58** 026013
- [67] Bortolon A, Camenen Y, Karpushov A N, Duval B P, Andrebe Y, Federspiel L and Sauter O 2013 Indirect measurement of poloidal rotation using inboard-outboard asymmetry of toroidal rotation and comparison with neoclassical predictions *Nucl. Fusion* **53** 023002
- [68] Crombé K *et al* 2005 Poloidal rotation dynamics, radial electric field, and neoclassical theory in the jet internal-transport-barrier region *Phys. Rev. Lett.* **95** 155003